



HAL
open science

Low-cycle fatigue crack initiation and propagation from controlled surface imperfections in nuclear steels

Paul Cussac, Catherine Gardin, Véronique Pelosin, Gilbert Hénaff, Laurent de Baglion, Olivier Ancelet, Stéphan Courtin

► **To cite this version:**

Paul Cussac, Catherine Gardin, Véronique Pelosin, Gilbert Hénaff, Laurent de Baglion, et al.. Low-cycle fatigue crack initiation and propagation from controlled surface imperfections in nuclear steels. *International Journal of Fatigue*, 2020, 139, pp.105703. 10.1016/j.ijfatigue.2020.105703 . hal-03763434

HAL Id: hal-03763434

<https://hal.science/hal-03763434>

Submitted on 30 Jan 2023

HAL is a multi-disciplinary open access archive for the deposit and dissemination of scientific research documents, whether they are published or not. The documents may come from teaching and research institutions in France or abroad, or from public or private research centers.

L'archive ouverte pluridisciplinaire **HAL**, est destinée au dépôt et à la diffusion de documents scientifiques de niveau recherche, publiés ou non, émanant des établissements d'enseignement et de recherche français ou étrangers, des laboratoires publics ou privés.

Low-cycle fatigue crack initiation and propagation from controlled surface imperfections in nuclear steels

International Journal of Fatigue, 2020, 139 : 105703

Cussac, P., C. Gardin, V. Pelosin, G. Hénauff, L. de Baglion, O. Ancelet, and S. Courtin

Abstract

The impact of a controlled surface imperfection on the low-cycle fatigue life in two different steels used in the French nuclear industry (304L austenitic stainless steel and 18MND5 low alloy steel) is investigated. After introduction of a single imperfection with a straight front and a depth varying from 50 to 350 μm in cylindrical samples, fatigue tests were conducted under fully-reversed total axial strain control in air at ambient temperature. It is shown that the fatigue life is significantly reduced, even in presence of small imperfections. In addition, the use of the potential drop methods provided an assesment of the initiation life and the determination of crack growth rates. Two characteristic crack growth domains were thus identified.

Corresponding author : catherine.gardin@ensma.fr

Keywords : Austenitic stainless steel; low-alloy steel; low-cycle fatigue; surface imperfection; fatigue life

Nomenclature

a	crack depth
a/b	ellipticity ratio or shape factor
b	ellipsis semi-major axis
D	specimen diameter
a/D	normalized crack depth
$\Delta\varepsilon_t$	total strain amplitude
DCPD	Direct Current Potential Drop
EDM	Electro Discharge Machining
N	lifetime in number of cycles
V	electrical potential difference
V_0	maximum value of V at the first cycle
V/ V_0	normalized electrical potential difference

1. Introduction

Given the stringent requirements of high levels of safety in nuclear components, stakeholders of the French nuclear industry must anticipate the potential occurrence of residual surface imperfections and justify the residual resistance of the concerned parts, in particular under cyclic loading. The surface anomalies considered in this context may be introduced at the end of manufacturing operations (finishing, marking, non-destructive testing) or during handling steps. Indeed, during these operations, surface defects, with a depth of a few tenths of a millimeter, can be generated during undesired events such as tool fall or friction, or during required and controlled operations, such as the positioning of slings. Generally, surface imperfections can act as initiation sites and as a consequence can affect the fatigue strength [1-4]. The issue of the fatigue strength of metal components in the presence of surface anomalies

41 has been the subject of a relatively large number of studies, but mainly in the high-cycle fatigue
42 regime [1, 3, 5]. For instance Inchekel and Talia [5] have studied the influence of scratches on
43 the fatigue resistance of an Al-Li alloy and have shown that their presence is highly detrimental
44 with a lifetime reduction close to 90% compared to those obtained on plain specimens. Cini and
45 Irving [3] have reached similar conclusions by studying the impact of the presence of scratches
46 on aluminium foil surfaces. They furthermore highlighted the influence of geometrical
47 parameters such as the scratch depth or root radius. A more recent study [1] has assessed the
48 effect of several types of surface imperfection on fatigue life in a nickel-base superalloy. These
49 authors more particularly evidenced the major influence of residual stresses generated during
50 the introduction of surface imperfections such as dents or scratches.

51 One of the major differences of the present study with respect to literature is that it is concerned
52 with low-cycle fatigue instead of high-cycle fatigue. Indeed, in addition to the thermal
53 fluctuations resulting from usual operating conditions, which are associated with stress
54 amplitudes below the fatigue limit, higher stresses can appear during transients. Such transients,
55 which correspond to power changes or unit start and restart, can generate thermal shocks
56 associated with large deformations inducing yielding.

57 The fatigue strength under large-scale plasticity in steels used in the nuclear industry has been
58 widely studied. Recent studies on 304L austenitic stainless steel have in particular addressed the
59 sensitivity of its fatigue resistance to various parameters such as the environment [6], the
60 loading type [7] or the surface finish [8-9]. For example, Poulain [8] has studied the effect of a
61 ground surface finish and has put forward that the induced surface roughness can not only affect
62 crack initiation, but also the first stages of propagation. Nevertheless, the impact of the presence
63 of a unique surface imperfection similar in shape to unintentionally generated scratches or dent,
64 under large-scale yielding conditions, has not been received a large attention so far on this type
65 of material.

66 The present study was undertaken in order to get a first assessment of the effect of surface
67 imperfections on the low-cycle fatigue resistance by considering two grades of steel typically
68 used in French nuclear power plants, namely an austenitic stainless steel 304L and a low-alloy
69 steel 18MND5 (equivalent to A533B). The selection of these two grades was supported by the
70 fact that the low-cycle fatigue of 304L is well documented in the authors groups, while it also
71 seemed interesting to conduct the same investigation in a grade with radically different
72 properties for comparison purposes. Besides, the surface imperfections considered here have to
73 be as close as possible from actual imperfections, that means characterized by a straight front,
74 a depth ranging between 100 and 350 μm , and a moderate notch root radius. However, for the
75 sake of conservatism of the approach, it was also decided not to take advantage of the possible
76 beneficial effect of compressive stresses which can be generated during the introduction of an
77 initial flaw like an impact or a scratch [1-2]. A special attention has thus been paid to develop
78 an experimental procedure to introduce surface imperfections that have to be reproducible,
79 representative of actual imperfections, free of residual stresses while giving rise to crack
80 initiation and propagation. With this aim, uniaxial low-cycle fatigue tests have been conducted
81 under total strain amplitude control on cylindrical samples containing an imperfection. In
82 addition, during the fatigue tests, the crack initiation and crack propagation stages have been
83 monitored by use of the direct current potential drop method (DCPD). This method requires the
84 prior determination of a calibration curve relating the potential measurements to the crack depth
85 and the reliability of the method strongly depends on the accuracy of this calibration. While

86 many techniques exist to calibrate the electrical potential evolution during crack propagation,
87 namely analytical [10-11] , analogical [10,12], numerical [13-16] and experimental [15, 17, 18],
88 in this study, an experimental calibration based on the use of ink markings has been established.

89 After a presentation of the aforementioned experimental methods, the low-cycle fatigue results
90 results obtained in both 304L and 18MND5 steels are detailed. The crack initiation and
91 propagation aspects are addressed.

92 **2. Materials and experimental methods**

93 *2.1. Materials description*

94 A 304L austenitic stainless steel and a low-alloy 18MND5 steel, respectively used for the
95 primary circuit pipes and the steam generators of the French nuclear power plants, have been
96 studied here. The 304L samples have been taken from a sheet obtained by rolling and having
97 undergone heat treatment at 1100°C followed by quenching with water. This treatment
98 guarantees the austenitic phase homogeneity at ambient temperature. The chemical composition
99 is given in table 1. The microstructure consists of an austenitic matrix dotted with residual
100 ferrite lamellas. The average size of grains is about 80 μm [19, 20].

Element	C	Cr	Ni	Si	Mn	S	P	Mo	Cu	N
Content (%)	0.029	18.00	10.0	0.37	1.86	0.004	0.029	0.04	0.02	0.056

101
102

Table 1 – 304L chemical composition [21]

103 The 18MND5 specimens have been taken from a steam generator shell section. The chemical
104 composition is given in table 2. Its good mechanical properties are due to the main following
105 alloying elements: manganese, nickel and molybdenum. The microstructure, of bainitic type,
106 consists of ferrite laths and carbides (cementite and molybdenum carbides). The prior austenite
107 grain size is close to 20 μm .

Element	C	Mn	Ni	Mo	Cr	Si	Cu	Al	V	S	P
Content (%)	0.18	1.55	0.71	0.5	0.16	0.21	0.04	0.02	0.02	0.001	0.007

108
109

Table 2 – 18MND5 chemical composition

110 *2.2. Specimen geometry and fatigue tests*

111 For both materials, the specimens have been machined by wire Electro-Discharge Machining
112 (EDM) and in such a way that the longitudinal axis of the specimens coincided with the rolling
113 direction for the 304L and the longitudinal steam generator shell axis for the 18MND5. The
114 specimens have a cylindrical shape with a 9 mm diameter and a 13.5 mm gauge length, as
115 shown in figure 1. All the specimens have been mirror-polished prior to testing in order to
116 unambiguously evidence the influence of surface imperfections.

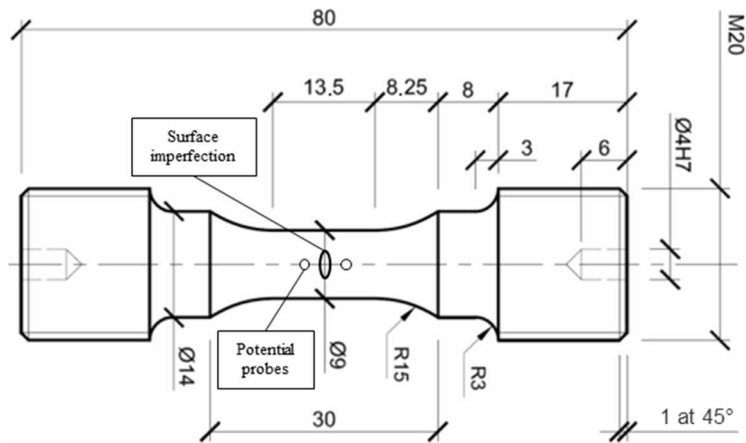


Figure 1 – Specimen geometry with surface imperfection and potential probes location

117

118

119 All the tests have been carried out at room temperature in laboratory air and under total strain
 120 amplitude control with a strain ratio $R_\epsilon = -1$. Strain was controlled using a remote extensometer
 121 with ceramic rods. Three strain amplitudes have been considered: $\Delta\epsilon_t / 2 = 0.2\%$, $\Delta\epsilon_t / 2 = 0.3\%$
 122 and $\Delta\epsilon_t / 2 = 0.6\%$. All the tests have been conducted on an Instron electromechanical fatigue
 123 machine equipped with a static 100 kN capacity load cell and adapted to cyclic load variations
 124 between -50 and +50 kN. The applied strain rate was kept constant and set at $0.4\% \times s^{-1}$. The
 125 resulting frequencies then varied between 0.167 and 0.5 Hz, depending on the strain amplitude
 126 considered. The tests are stopped on the basis of a load drop criteria, the lifetimes considered
 127 in the framework of this study are associated with a 5% drop in the stabilized stress and are
 128 noted N_5 .

129 Most of the tests have been carried out on specimens containing a surface imperfection. A
 130 unique imperfection was introduced per specimen. The imperfection was systematically placed
 131 in the center of the specimen gauge (figure 1) and perpendicular to the stress axis, so as to
 132 introduce a mode I loading for the crack initiated from the imperfection, which is recognized
 133 as being the most unfavorable case for fatigue crack growth.

134 2.3. Introduction of the surface imperfections

135 Two methods have been used for machining surface imperfections:

- 136 - A sinker electro-discharge machining (EDM) process based on the use of electrodes made of
 137 copper and designed to obtain sharp artificial notches;
- 138 - An “abrasive machine” which has been developed by the Pprime Institute in the context of
 139 previous studies [1,16] and which consists in a gradual removal of material by abrasion using
 140 a ceramic disc and a diamond powder. In order to get sharp imperfections like those introduced
 141 by the EDM method, the abrasive machine disk is previously sharpened.

142 The choice of these two processes is related, first, to the good geometrical reproducibility of
 143 the surface imperfections obtained but also, as we care about conservatism, to the need to limit
 144 the compressive residual stresses at the bottom of the imperfections. Actually, it is well known
 145 that this kind of stress generally delays crack initiation and propagation [1-2]. The imperfections
 146 artificially introduced in this study cover a range of depths from approximately 50 to 350 μm .
 147 Geometric characteristics of all the imperfections have been systematically analyzed by means
 148 of an optical microscope. The imperfection length and width depend on the depth and vary

149 respectively from approximately 1.5 to 3.5 mm and from 200 to 400 μm . The average opening
150 angle and notch root radius are respectively 40° and $80 \mu\text{m}$.

151 *2.4. Crack initiation and growth monitoring : DCPD technique and ink markings*

152 The Direct Current Potential Drop monitoring method, also known as DCPD, was implemented
153 to monitor the initiation and propagation of cracks during tests. It consists in introducing a direct
154 current through a specimen and in measuring the potential value on both sides of the crack.
155 During crack growth, the electrical resistance rises and causes, in accordance with Ohm's law,
156 an increase in the potential difference between the measurement points. It is then possible to
157 monitor in real-time the crack growth. The use of this technique has been possible thanks to the
158 damage localization induced by the presence of the surface imperfection. Indeed, the
159 implementation of potential monitoring requires the prior knowledge of the crack initiation
160 location in order to place the potential probes. In this study, the main crack has systematically
161 initiated from artificially introduced surface defects. The electrical current is introduced into
162 the samples by means of wires connected to the machine grip lines. The latter has been
163 previously isolated from the rest of the machine frame by means of insulating sheets to prevent
164 electrical interference and to limit the noise in the potential signal. In order to reduce the
165 specimen heating by Joule effect, which could influence the potential measurement, the current
166 is introduced per pulse ($I_{\min} = 0$ and $I_{\max} = 1 \text{ A}$) at a 100 Hz frequency. The electrical voltage,
167 denoted V , is measured by means of 0.1 mm diameter platinum wires which are spot-welded at
168 a distance of 1 mm from the defect center. In order to ensure that the measurement is
169 independent of material properties, V is normalized using the value measured at the first cycle
170 maximum, denoted V_0 . This formalism also enables to take into account the plastic deformation
171 occurring at the beginning of the test and which may influence the measurement of the potential
172 [22-24].

173 However, this technique requires to determine a reliable calibration curve connecting the
174 measured potential difference to the crack depth.

175 The ink marking technique has been selected to visualize the crack fronts at different steps
176 during propagation. This technique is inexpensive and easy to implement, and it furthermore
177 gives satisfying results in the conditions examined here (tests in laboratory air at room
178 temperature). The inks used are fast-drying acrylic and are commercially purchased. By the use
179 of different ink colors during a test, several markings can be performed on the same fracture
180 surface.

181 The principle of this method is to apply ink directly on the specimen surface near the surface
182 imperfection by using a brush. This very fast operation is followed by a phase of removal of
183 the ink in excess at the surface. The markings are realized without stopping the tests, allowing
184 a better ink penetration during the crack opening phase. The operation is carried out during a
185 few cycles only (between 2 and 10 approximately, depending on the test frequency) and the
186 rapid drying of the ink limits its spread after application.

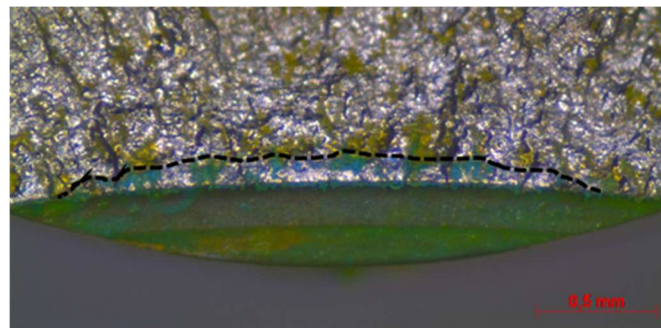
187

188 **3. Experimental results**

189 *3.1. Calibration of the Direct Current Potential Drop method*

190 *3.1.1. Crack initiation threshold*

191 One of the first challenges in calibrating electrical potential monitoring is to be able to identify
192 a threshold above which a crack initiated from the initial imperfection is assumed to propagate.
193 In order to evidence an initiation threshold, several markings were made on 304L specimens,
194 for different relative values of the electrical potential difference. The analysis of these markings
195 according to the applied strain or the initial imperfection depth has shown that those parameters
196 have no significant influence on the initiation threshold. The ink markings performed on 304L
197 steel have revealed that a 1% variation in the normalized potential difference can be associated
198 with a crack depth close to 100 μm . One ink marking performed onto a 18MND5 sample (figure
199 2) has confirmed this value. Consequently, the 1% potential variation has been considered as
200 the threshold for crack initiation in both materials in the subsequent tests. This initiation
201 threshold definition has been subsequently used to analyze experimental data resulting from
202 fatigue tests. One can note that it is consistent with the grain size in 304L which is close to 80
203 μm on average. This order of magnitude for the initiation threshold (100 μm depth) has been
204 used by some authors [1,25].

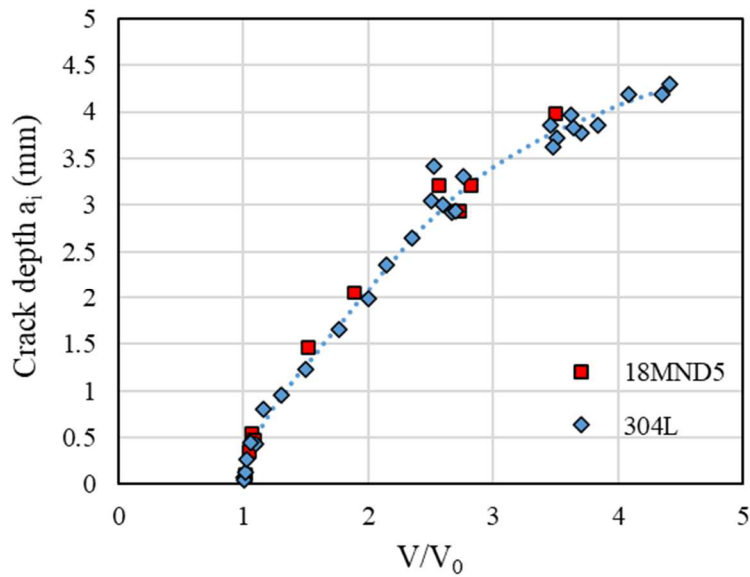


205

206 **Figure 2 - Ink marking in a 18MND5 specimen associated with a crack propagation close to 100 μm in**
207 **depth**

208 *3.1.2. Calibration of the electric potential method*

209 The experimental calibration of the electrical potential crack growth monitoring is based on the
210 observation of the fracture surfaces after completion of the fatigue tests. The use of a relatively
211 large number of ink markings permitted to characterize the propagation. Indeed, based on these
212 markings but also on the final crack fronts, it is possible to observe several crack propagation
213 stages on the same fracture surface. All the collected information was used, by associating each
214 marking and crack front with a given experimental potential value, to experimentally
215 reconstruct the crack depth variation as a function of the potential difference evolution as shown
216 in figure 3. Experimental data generated for both materials are represented on this curve without
217 distinction of the test conditions in terms of applied strain amplitude or initial notch geometry.
218 Furthermore the crack depth value considered in this figure is the maximum depth at the center
219 of the test sample by taking as a reference the notch root (a_i in figure 7). In other words, only
220 the propagated part of the crack is taken into account here.



221

222 **Figure 3 - Crack depth as a function of the normalized potential difference for both 304L and 18MND5**
 223 **steels.**

224 No influence of the various test parameters can be noticed here. Hence, the total strain
 225 amplitude, the initial surface imperfection depth or the material do not affect the electrical
 226 potential variation in the framework of this study. This result can be partly explained by the use
 227 of a reference potential V_0 which, in particular, allows to get free of the material electric
 228 properties. In order to use the calibration data continuously, an interpolation of the 304L data
 229 was performed (dashed line in figure 3).

230 **3.2. Crack initiation from surface imperfection**

231 **3.2.1. Crack initiation observations**

232 In fatigue tests carried out on specimens containing a surface imperfection, the initiation of the
 233 main crack systematically occurred from this imperfection. More specifically, whatever the
 234 strain level or the imperfection depth and type considered, optical observations carried out
 235 during the tests by means of a long focal length microscope, have revealed a systematic
 236 initiation in the center and at the root of the defects. These zones correspond to the maximum
 237 surface imperfection depth and are associated with a significant deformation concentration. An
 238 example of a crack initiated at an imperfection root is shown in figure 4.

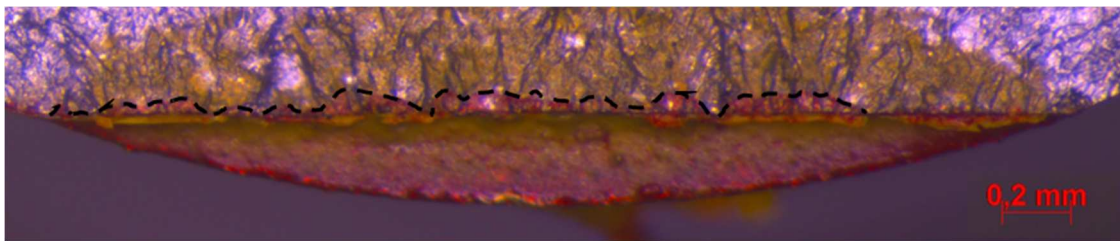


239

240 **Figure 4 - Initiation and propagation of a crack from a surface imperfection at $\Delta\epsilon_t/2 = 0.6\%$ (18MND5)**

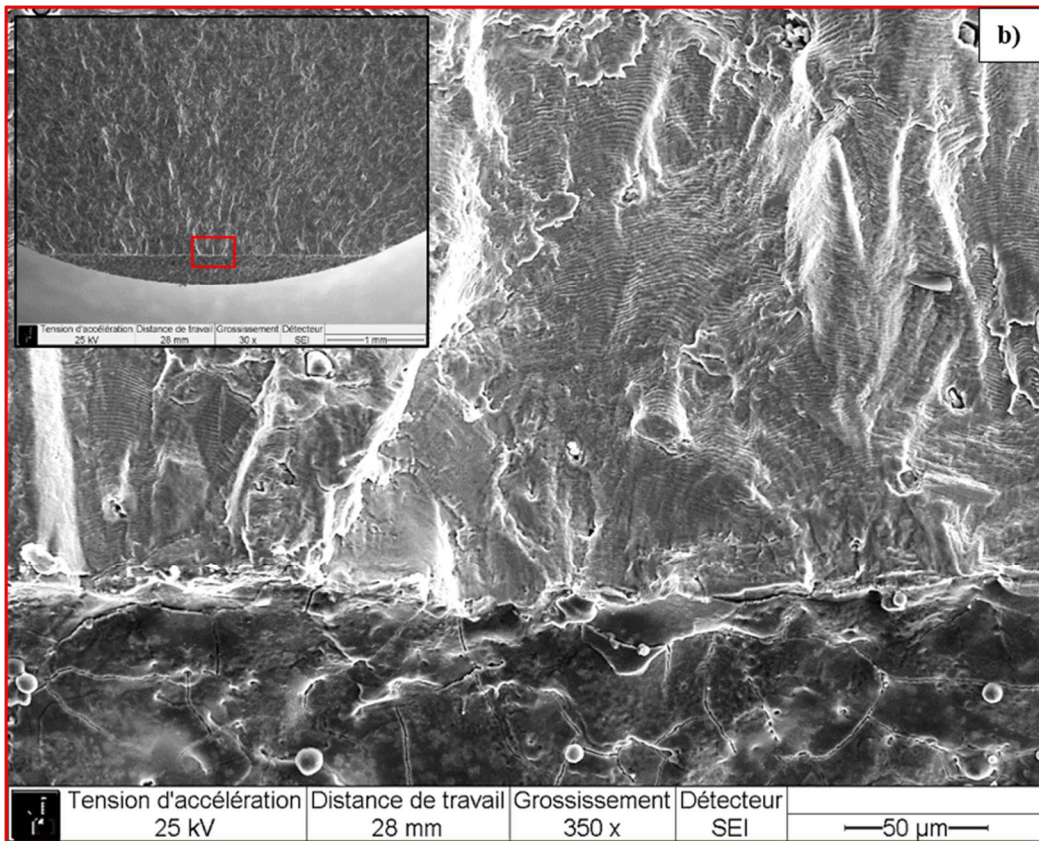
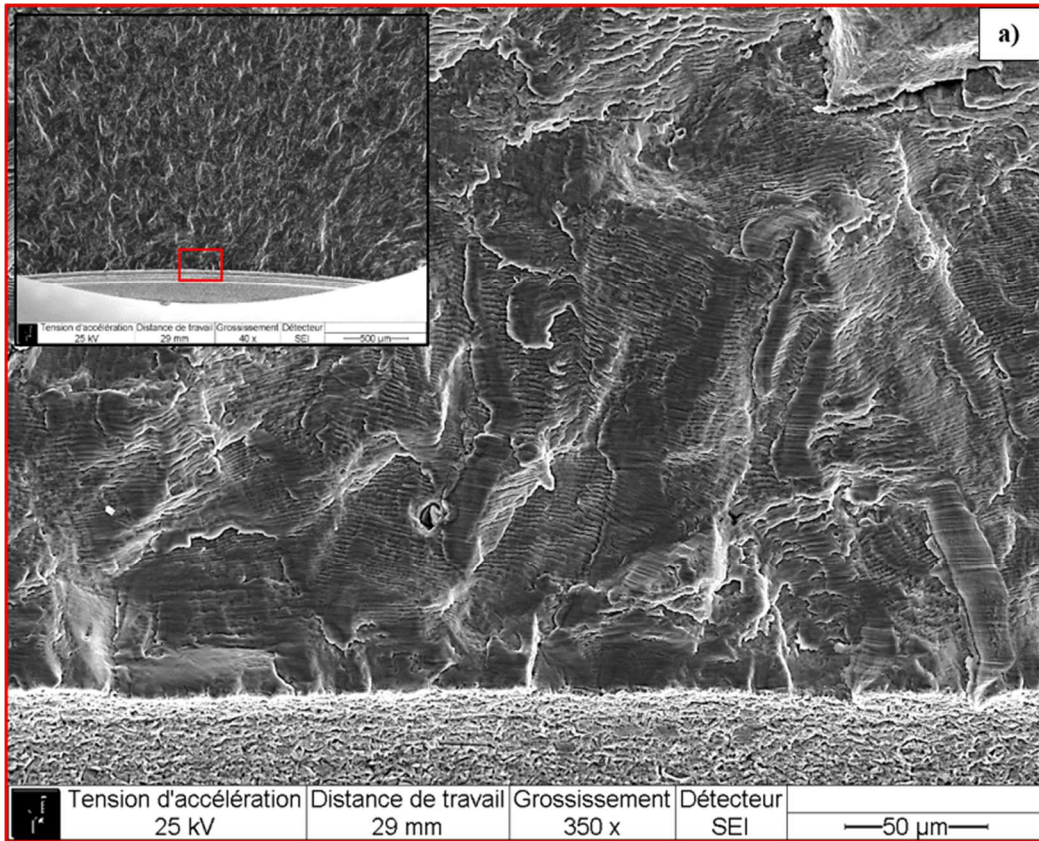
241 Fracture surface analysis performed by Scanning Electron Microscopy (SEM) and optical
242 microscopy shows that multi-cracking can occur (figures 5-6). In fact, multiple micro-cracks
243 can initiate at different locations along the notch root and quickly coalesce to form a single
244 crack encompassing the entire length of the notch root. Such an example of multi-cracking is
245 given in figure 5 with the first ink marking represented in this figure with the dotted line and
246 corresponding to an advancement of 3% in the lifetime. First, as illustrated in figure 6, the river
247 lines on the fracture surface demonstrate that there is not a single initiation site since they do
248 not converge to a specific location, but rather seem to originate from several locations along
249 the imperfection root. Moreover, striations visible in figure 6.a exhibit different propagation
250 directions, which also suggest the presence of several initiation positions. In some cases, multi-
251 cracking has been observed with the formation of cracks in distinct planes. Nevertheless, this
252 phenomenon could not be associated with a particular surface condition. Furthermore, it should
253 be noticed that, irrespective of the test conditions, the imperfection edges do not appear as
254 privileged initiation sites.

255 Finally no significant differences in the crack initiation mode have been identified according to
256 the defect type. Only the imperfection flanks differ with the presence of microcracks on EDM
257 ones (figure 6.b) in contrast to abrasive-type defects which do not display any sign of damage.



258

259 **Figure 5 - Optical microscopy example of crack initiation from fracture surface presenting ink markings -**
260 **Initial surface imperfection made by EDM (Depth = 280 μm , $\Delta\epsilon_t/2 = 0.6\%$; 304L)**



263 **Figure 6 - 304L fracture surface analysis by SEM - a) Potential initiation site from abrasive machine**
 264 **imperfection ; b) potential initiation site from EDM imperfection**

265 *3.2.2. Crack initiation stage*

266 All experimental data obtained from the electrical potential monitoring have been analyzed
 267 using the previously defined threshold value associated with a crack propagation distance of
 268 about 100 μm ($V/V_0 = 1.01$). For each test performed, this allows to assess the crack initiation
 269 duration, called $N_{\text{initiation}}$. The results obtained for both 304L and 18MND5 steels at the different
 270 strain amplitudes are listed in table 3. The fatigue lifetime of each specimen is also recorded in
 271 this table. The lifetime considered here, noted N_5 , corresponds, as mentioned in the section 2.2,
 272 to a 5% decrease from the stabilized stress.

Material	$\Delta\epsilon_i/2$	Imperfection type	Imperfection depth (micrometers)	N_5 (cycles)	$N_{\text{initiation}}$ (cycles)	Proportion of crack initiation
304L	0.2%	EDM	110	19 100	2 800	15%
		Abrasive machine	110	27 300	6 500	24%
		Abrasive machine	220	16 610	1 120	7%
		EDM	320	10 200	400	4%
		Abrasive machine	320	12 000	1 000	8%
	0.3%	Abrasive machine	120	7 710	910	12%
		Abrasive machine	180	7 550	1 280	17%
		Abrasive machine	350	3 800	290	8%
	0.6%	Abrasive machine	110	1 750	300	17%
		EDM	170	1 500	220	15%
		EDM	280	910	30	3%
		Abrasive machine	280	970	110	11%
		Abrasive machine	290	910	70	8%
		EDM	310	840	80	10%
	18MND5	0.2%	Abrasive machine	50	66 900	21 810
Abrasive machine			140	42 940	2 580	6%
Abrasive machine			270	19 150	1 510	8%
0.6%		Abrasive machine	130	1 010	70	7%
		Abrasive machine	220	620	90	15%
		Abrasive machine	330	610	60	10%

273 **Table 3 - Fatigue lifetimes and initiation duration for 304L and 18MND5 steels**

275 In the case of the 304L steel, whatever the strain level considered, the fraction of the total life
 276 consumed during crack initiation is relatively small in the presence of a surface imperfection.
 277 The proportion of crack initiation in the total lifetime varies from 3 to 24% maximum.
 278 Regardless of the imperfection depth, it can also be noticed that the strain amplitude, as
 279 expected, plays a major role on initiation duration in absolute value, the latter decreasing
 280 sensibly when the strain level increases. Furthermore, the influence of the imperfection depth
 281 and type can be noted. Indeed, the number of cycle to initiation tends to decrease along with
 282 the increase in crack depth. As an example, at $\Delta\epsilon_i/2 = 0.6\%$, $N_{\text{initiation}} = 300$ cycles for an initial
 283 imperfection depth of 110 μm while it represents only 90 cycles for a 290 μm initial depth. One
 284 can notice that in some cases, this trend is not always respected, especially when the
 285 imperfection type considered differs. Actually, at equivalent depths and strain amplitude, the
 286 EDM type imperfections can be associated with lower initiation times. The influence of the
 287 imperfection type and depth on the 304L steel is discussed in particular in the section 4.1.

288 In the case of the 18MND5 steel, the initiation in the presence of imperfection represents
 289 between 6 and 33% of the total lifetime N_5 . As for the stainless steel, the initiation times are

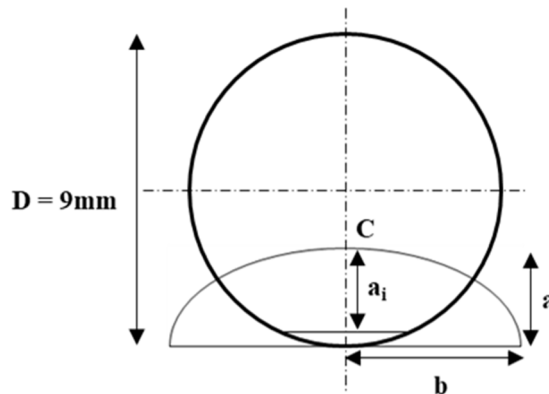
290 strongly reduced in absolute value for the higher applied strain amplitude. However, when
 291 considering the proportion of crack initiation, the results does not exhibit any significant effect
 292 of the strain amplitude. Besides, an analysis of the data according to the crack depth shows that,
 293 in the frame of the depth considered for this material, this latter parameter does not have a
 294 particular impact on the crack initiation except for the lowest depth, namely 50 μm . Actually,
 295 in a depth interval included between 130 and 330 μm , the relative crack initiation times remain
 296 close to 10% and vary only from 6 to 15%. This result suggests that from a certain depth level,
 297 no significant changes in the proportion of crack initiation should be expected on this material.

298 Eventually, in the presence of a surface imperfection, regardless of its depth or type, cracks
 299 initiate very rapidly, meaning that most of the fatigue lifetime is represented by the propagation
 300 stage. The analysis of this phase is therefore of particular importance and is addressed in the
 301 next sections.

302 3.3. Fatigue crack propagation analysis

303 3.3.1. Crack front shape evolution

304 The fracture surface observations have also enabled to reconstruct the crack propagation history
 305 from surface imperfections by analyzing ink markings and crack front shapes corresponding to
 306 the end of the tests. After the initiation stage described in the previous section, it is noticed that
 307 the crack front quickly evolves into a semi-elliptical shape that can be described by two
 308 characteristic parameters a and b . Figure 7 introduces the convention that was adopted during
 309 this study to analyze the crack shape evolution. The quantity a corresponds to the crack depth
 310 measured from the specimen surface to point C (this distance is also called semi-minor axis of
 311 the ellipse) and b is assimilated to the semi-major axis, then, a/b is the ellipticity ratio.



312

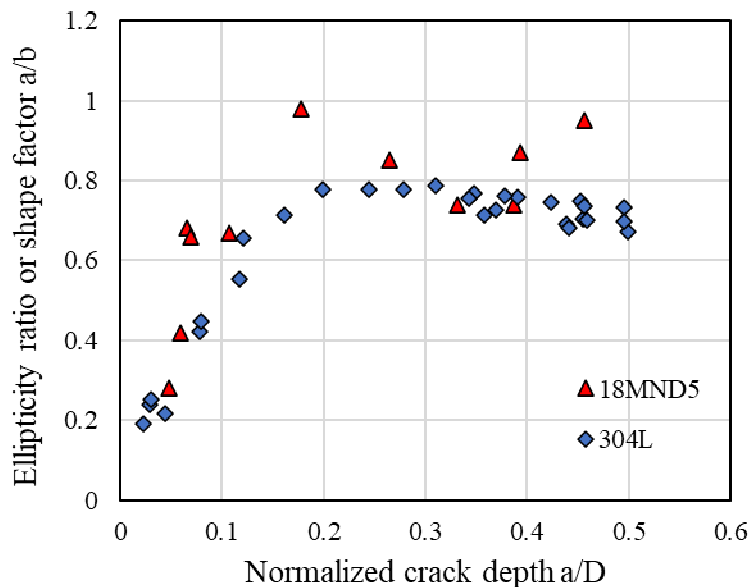
313 **Figure 7 - Semi-elliptical crack front characterized by the parameters a (crack depth from the surface)**
 314 **and b (semi-major axis of the ellipse) ; a_i (crack depth from the notch root)**

315 Case of 304L

316 For 304L, during crack propagation, the crack front retains a semi-elliptical shape. It starts with
 317 an elongated shape (low a/b ratio) and then evolves towards a circular one (a/b increases) before
 318 stabilizing around a shape having an ellipticity ratio close to 0.7. Figure 8 shows the evolution
 319 of this ratio as a function of the dimensionless value a/D (crack depth a divided by the specimen
 320 diameter D whose value is 9 mm). The analysis of the experimental points presented in figure
 321 8 according to the applied strain amplitude or the initial defect depth demonstrates that these
 322 two parameters have no influence on the crack front shape evolution. However, given the
 323 relatively limited number of data points and the analysis of fracture surfaces, the crack front

324 shape may slightly differ from one defect to another one in the early stages of propagation.
 325 Indeed, during the initiation and the beginning of micropropagation stage, the hypothesis of a
 326 semi-elliptical crack is not valid. As shown in the previous section (figure 5), the crack does
 327 not immediately satisfy the semi-elliptical crack shape assumption, with an initial irregular
 328 shape. Thus, the very first points in figure 8 must be considered with care as, in this propagation
 329 domain, the assumption of a semi-elliptical crack is not fully consistent with experimental
 330 observations.

331 Beyond initiation and early stages of propagation, generally, once the crack has begun to
 332 propagate on the specimen edge, getting out of the initial defect, the semi-elliptical crack front
 333 assumption is systematically respected, and the influence of the initial defect appears to be
 334 negligible. This result is also consistent with literature data from Carpinteri [26]. This author
 335 has actually modeled the crack front shape evolution in a round bar from initial cracks
 336 presenting different geometric characteristics. The conclusions from Carpinteri highlight a
 337 convergence of the crack shape towards an a/b ratio close to 0.6 independently of the initial
 338 conditions, in consistency with the results presented here.

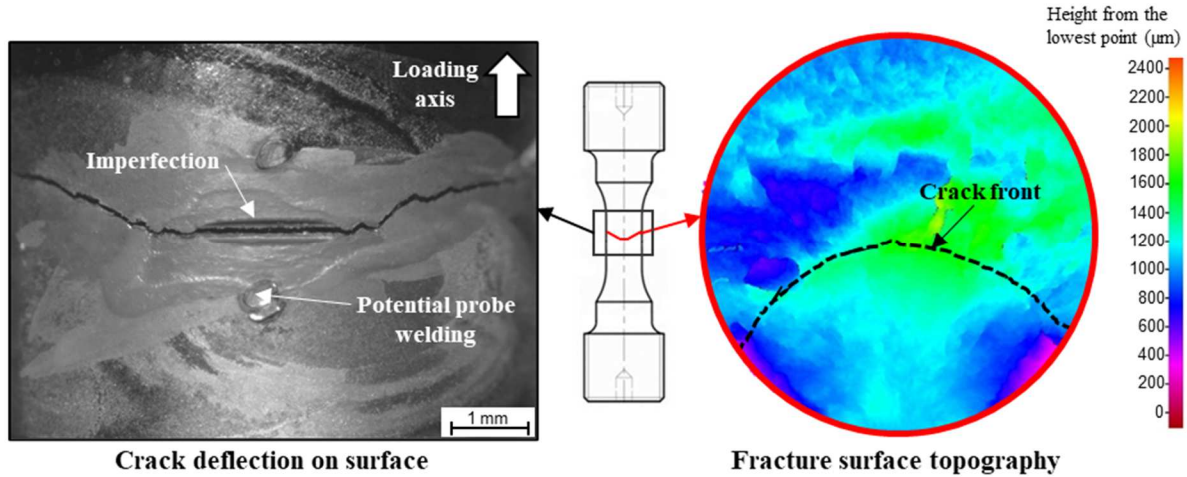


339
 340 **Figure 8 - Evolution of the a/b ratio determined experimentally from the fracture surfaces analysis for**
 341 **both 304L and 18MND5 steels**

342 *Case of 18MND5*

343 Despite a relatively large scatter, the evolution of the crack front shape in 18MND5 steel is
 344 similar to the one observed in 304L steel. Thus, after initiation, the crack front, which has an
 345 initially elongated shape, rapidly evolves into a more circular one. A few points deviate
 346 however from the general trend and correspond with values of the a/b ratio close to 1. The
 347 discrepancy observed could be attributed to the crack deflection systematically observed on the
 348 sample surfaces. One example of such crack deviation upon the specimen barrel is shown in
 349 figure 9. Actually, the crack front shape considered for the determination of the a/b ratio
 350 corresponds to a projection onto a propagation plane viewed as perpendicular to the loading
 351 axis. The consideration of the real crack front would tend to increase the value of the semi-
 352 major axis b and consequently to decrease the one of the a/b ratio which would thus become
 353 closer to those observed on the 304L steel. Moreover, a topographic analysis has been

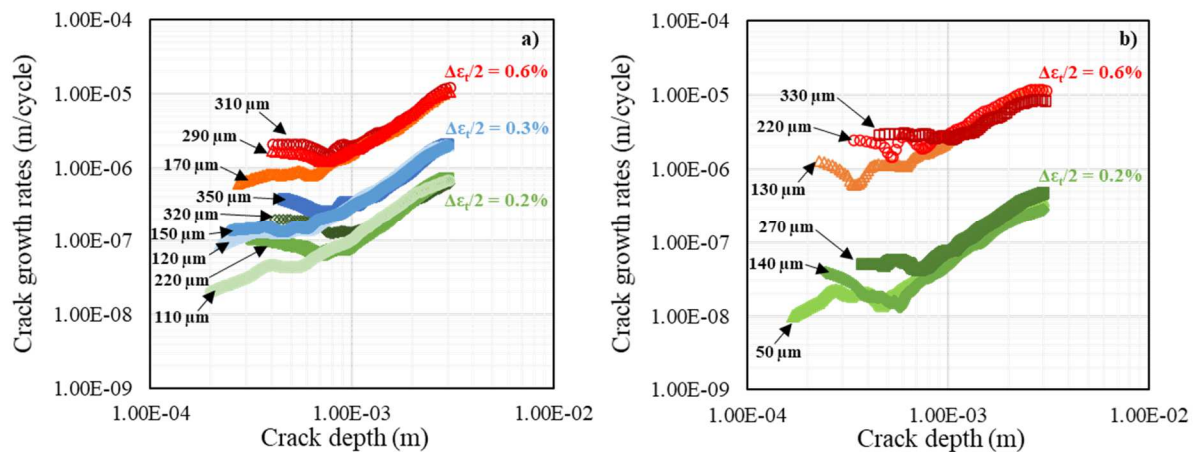
354 performed (figure 9) and shows that the deflection is only effective in the immediate vicinity
 355 of the specimen edges and, in the fracture surface center, the crack lips remain flat. Eventually,
 356 while the crack deflection could potentially explain the particular crack front shape recorded on
 357 this material, further investigations should be undertaken in order to validate or not this
 358 hypothesis and understand the origin of this phenomenon.



359
 360 **Figure 9 - Illustration of the crack deflection occurring on 18MND5 steel specimens - Crack deflection at**
 361 **the specimen surface (on the left) ; Topographic analysis by optical microscopy of the fracture surface (on**
 362 **the right)**

363 *3.3.2. Fatigue crack growth rates derived from DCPD measurements*

364 The fatigue crack growth rates derived from the electrical potential tracking analysis using the
 365 calibration curve previously established are represented as a function of the crack depth in
 366 figure 10, for the various strain amplitudes studied.



367
 368 **Figure 10 – Fatigue crack growth rates as a function of crack depth - a) 304L ; b) 18MND5 (Initial**
 369 **imperfection depths are indicated with arrows)**

370 *Case of 304L*

371 The crack propagation rates appear to be strongly dependent on the strain level as shown in
 372 figure 10.a. Indeed, for a total strain amplitude of 0.2%, fatigue crack propagation rates range
 373 from 2×10^{-8} to 7.2×10^{-7} m/cycle while at $\Delta \epsilon_t/2 = 0.3\%$ strain level, they range from 1×10^{-7} to

374 2×10^{-6} m/cycle and at last, they vary from 4×10^{-7} to 1.5×10^{-5} m/cycle at the highest strain level
375 $\Delta \varepsilon_t/2 = 0.6\%$.

376 Regardless of the strain amplitude or the imperfection depth considered, the evolution of fatigue
377 crack propagation rates can be systematically divided into two parts. Thus, in the first part of
378 the curves corresponding to depths from the initiation threshold to depths varying
379 approximately between 0.6 and 1.3 mm maximum (according to the initial imperfection), the
380 crack propagation rates present a pseudo-plateau behaviour, with a relatively small increase, or
381 even a decrease, and undergo significant fluctuations. Moreover, this propagation domain
382 seems to be very dependent on the initial imperfection depth. Indeed, the deeper the initial notch
383 is, the higher the initial crack propagation rates are.

384 Beyond a certain threshold in terms of crack depth, which seems to depend on the imperfection
385 depth considered, fatigue crack propagation rates from different tests tend to merge along a
386 unique curve, which will be associated here to a steady-state crack propagation regime. In this
387 domain, the increase in crack growth rates as a function of crack depth is independent of both
388 strain amplitude and initial imperfection depth and seems to evolve as a power-type function.
389 At the end of the curves, one can notice a slope change which is characterised by a reduction in
390 the rate of increase. This effect can be attributed to the significant damage present in the
391 specimen at the end of the test, contributing significantly to its deformation and leading to crack
392 driving force drop.

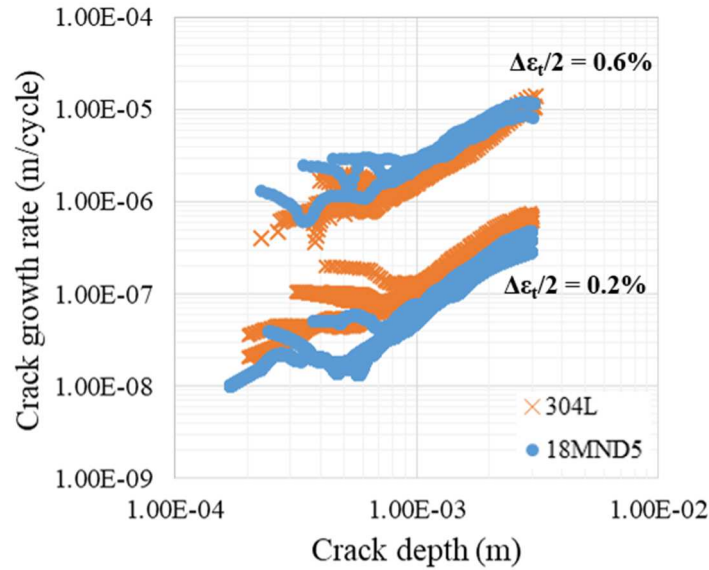
393 *Case of 18MND5*

394 In the low alloy steel 18MND5, fatigue crack propagation rates are once again controlled by
395 the strain amplitudes: an increase in the strain amplitude leads to a substantial increase in crack
396 growth rates. At $\Delta \varepsilon_t/2 = 0.2\%$, crack propagation rates observed range from about 1×10^{-8} to
397 5×10^{-7} m/cycle while the range is from 1×10^{-6} to 1×10^{-5} m/cycle at $\Delta \varepsilon_t/2 = 0.6\%$.

398 As for 304L material, two propagation stages can be observed on this material, regardless of
399 the strain level considered. Once again, the first propagation stage is characterized by a strong
400 dependence on the initial imperfection depth and is still associated with significant fluctuations.
401 The dependency of growth rates on initial surface imperfections also follows the same trend as
402 observed on the 304L: the initial fatigue crack propagation rates increase with the imperfection
403 depth. Above a threshold (comparable with the ones observed on the 304L), also depending on
404 the notch depth, a change in the propagation regime occurs. The crack growth becomes
405 independent of the initial imperfection and is only governed by the applied strain amplitude. In
406 the same way, as for the stainless steel and for similar reasons, a drop in the crack driving force
407 can also be observed at the end of the curves.

408 *Crack growth rate comparison between 304L and 18MND5*

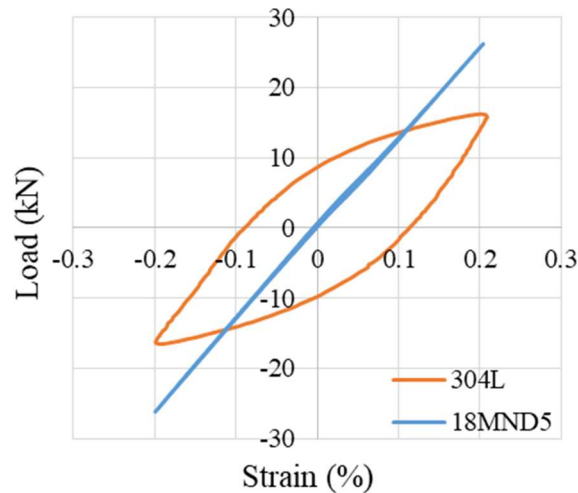
409 A comparison of the evolution of fatigue crack propagation velocities for 304L and 18MND5
410 steels is proposed in figure 11. Crack growth rates associated with 304L steel are higher than
411 those of 18MND5 at $\Delta \varepsilon_t/2 = 0.2\%$ on the whole propagation range. However, the differences
412 are particularly marked in the micropropagation domain. For the highest strain level, at $\Delta \varepsilon_t/2 =$
413 0.6% , the growth rates are generally very close, although those associated with stainless steel
414 appear to be slightly lower.



415

416 **Figure 11 - Comparison of both 304L and 18MND5 crack growth rates derivated from potential**
 417 **monitoring analysis at $\Delta\epsilon_t/2 = 0.2\%$ and $\Delta\epsilon_t/2 = 0.6\%$**

418 The important differences in velocities observed at $\Delta\epsilon_t/2 = 0.2\%$, especially in the first
 419 propagation domain, are partly linked to the highly dissimilar plasticity levels at this strain
 420 amplitude between these two steels. Indeed, the higher crack propagation rates on the 304L
 421 could derived from the significant plasticity occurrence at low strain amplitude, contrary to the
 422 18MND5 (figure 12). This generalized plasticity is likely to assist the crack propagation and
 423 thus to promote higher velocities.



424

425 **Figure 12 - Comparison of 304L and 18MND5 hysteresis loop at $\Delta\epsilon_t/2 = 0.2\%$**

426

427 **3.4. Influence of surface imperfections on fatigue strength**

428 In this section, the influence of surface imperfections on the fatigue strength is studied through
 429 an analysis of the relative lifetime evolution as a function of the initial defect depth. The relative
 430 lifetime corresponds to the ratio of the lifetime in the presence of a defect to the reference
 431 lifetime associated with virgin specimens. The fatigue lifetimes considered here are the
 432 previously defined N_5 lifetime and the lifetimes derived from the ANL (Argonne National

433 Laboratory) equations presented below. Indeed, in the framework of this study, only one
 434 reference test (without imperfection) has been performed for each strain amplitude, the use of
 435 ANL equations as reference allows to overcome the natural scatter which may be associated to
 436 these tests. The ANL fatigue lives, noted here N_{ANL} , are provided from equations 1 and 2 for
 437 the low alloy steels and from equations 3 for the austenitic stainless steels. These equations are
 438 derived from fatigue life models for estimating the fatigue lives in air based on the existing
 439 fatigue ϵ -N data at ANL as best-fits of a Langer curve to the data [27].

440 Equations 1 and 2 provide the ANL fatigue life for low alloy steel in air at a given temperature
 441 T:

$$442 \quad \ln(N_{ANL}) = 6.480 - 0.00124T - 1.808 \ln(\epsilon_a - 0.151) \quad (1)$$

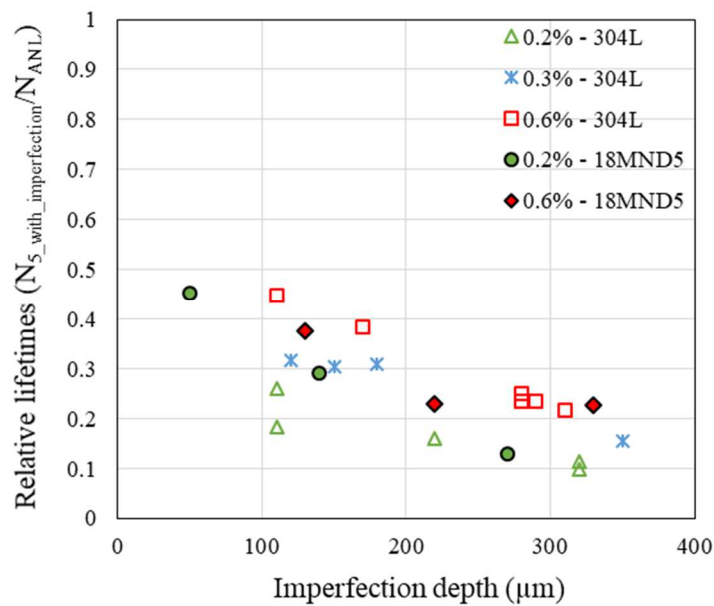
443 Thus, in room temperature the equation (1) is expressed as:

$$444 \quad \ln(N_{ANL}) = 6.449 - 1.808 \ln(\epsilon_a - 0.151) \quad (2)$$

445 Equation 3 gives the ANL fatigue life for austenitic stainless steel in air at temperatures up to
 446 400°C:

$$447 \quad \ln(N_{ANL}) = 6.891 - 1.92 \times \ln(\epsilon_a - 0.112) \quad (3)$$

448 Where N_{ANL} is the fatigue life in cycles, ϵ_a the strain amplitude and T the test temperature (°C).



449

450 **Figure 13 - Evolution of the relative lifetime as a function of imperfection depth for 304L and 18MND5**

451 Regardless of the material or strain amplitude considered, it can be seen in figure 13 that fatigue
 452 life is strongly affected by the presence of a surface imperfection. Indeed, even in presence of
 453 shallow imperfections whose depths are close to 50 or 100 µm, a significant reduction in fatigue
 454 strength is noticed. Furthermore, the results presented in figure 13 highlight the influence of the
 455 imperfection depth which appears to be the main parameter governing the fatigue life. The
 456 analysis of lifetime evolution as a function of other geometric parameters such as the opening
 457 angle or the notch tip radius does not reveal any particular trend whatever the material or strain
 458 level considered. This result is consistent with the works of several authors [3,5] who have
 459 studied the influence of surface imperfection such as scratches.

460 Besides, the data analysis associated with the 304L steel also suggests that the surface
 461 imperfection effect on fatigue strength could depend on the strain amplitude. Actually, at
 462 equivalent depth, the presence of a surface imperfection seems to be more harmful at low strain
 463 levels, especially for the lowest value, $\Delta\varepsilon_f/2 = 0.2\%$. In the low alloy steel 18MND5, no
 464 particular influence of the strain level can be put forward in the limited data set.

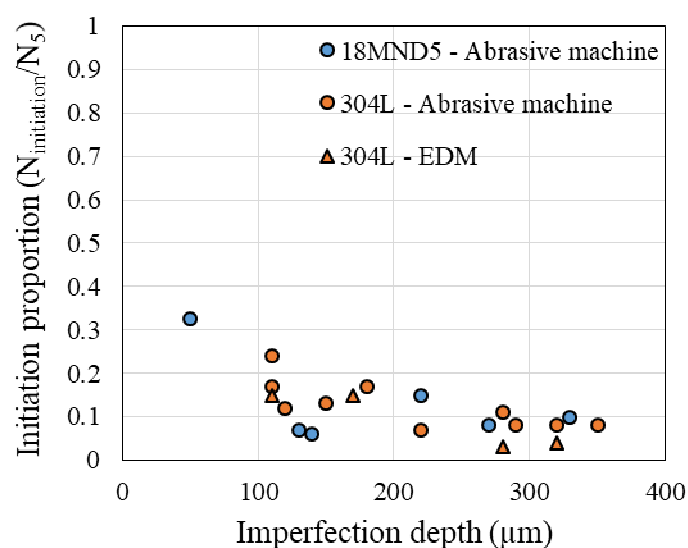
465 The comparative analysis in figure 13 does not evidence any particular difference in the
 466 sensitivity of these two steels to the presence of imperfections. In fact, their influence does not
 467 seem, in the test conditions examined, to be more pronounced in either of the two materials,
 468 despite of their difference in microstructure and associated mechanical properties.
 469 Nevertheless, a closer look at the results according to the strain amplitudes indicates that
 470 18MND5 could be slightly less sensitive to the presence of imperfection at the lowest strain
 471 level, namely $\Delta\varepsilon_f/2 = 0.2\%$. Indeed, for the first two points, associated with depths of 50 and
 472 140 μm , the relative lifetimes appear to be higher than those that would be obtained, at equal
 473 depths, on 304L. This difference between the two materials could possibly come from the
 474 radically different amount of cyclic plasticity generated for a given total strain amplitude (see
 475 figure 12). The aforementioned trends regarding the 18MND5 steel should nevertheless be
 476 considered cautiously due to the limited number of experimental points available for this
 477 material.

478

479 4. Discussion

480 4.1. Crack initiation from surface imperfection

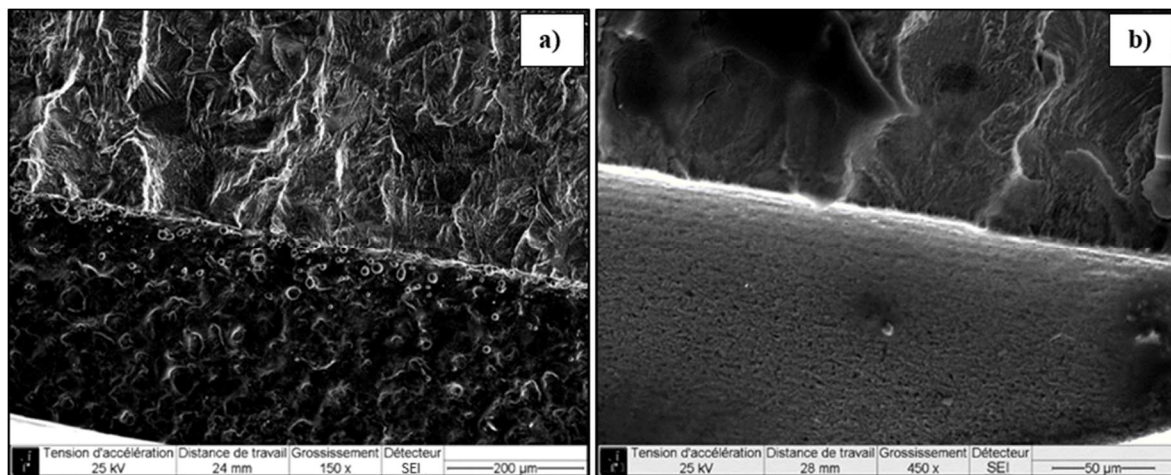
481 It has previously been shown (section 3.2.2) that the imperfection depth and type of machining
 482 (abrasive machine and EDM) can affect the initiation durations. An analysis of the proportion
 483 of fatigue life devoted to crack initiation, represented by the ratio $N_{\text{initiation}}/N_5$, as a function of
 484 the initial imperfection depth is provided for both 304L and 18MND5 in figure 14. Results are
 485 also distinguished according to the imperfection type (EDM or abrasive machine).



486

487 **Figure 14 - Evolution of the relative crack initiation time according to the initial imperfection depth**

488 For the two materials studied here, figure 14 illustrates that the relative initiation times tend to
 489 decrease with the rise of the surface imperfection depth. In the 304L steel, for imperfections
 490 whose depths are close to 100 μm , the proportion of crack initiation lifetime varies from 15 to
 491 24%, while it ranges from 3 to 11% for imperfections with depths close to 300 μm . The
 492 variations observed in this material at equivalent depths may be due to the type of imperfection.
 493 Indeed, the electroerosion process seems to favour a faster initiation compared to the abrasive
 494 machine. Two reasons can mainly be put forward to explain these differences between the two
 495 imperfection types. First, the surface finish associated with EDM-type imperfections has a
 496 much more pronounced roughness than the one observed on abrasive machine imperfections
 497 (figure 15). Some studies, conducted on 304L steel [8-9], have demonstrated the significant
 498 effect of this parameter on fatigue crack initiation. In addition, because of its nature and unlike
 499 the abrasive machine, the electroerosion process strongly interacts with the material by creating
 500 a heat-affected zone which may also contribute to a faster initiation. Finally, the use of copper
 501 electrodes for machining EDM-type imperfections can potentially induce local copper
 502 contamination which could also influence the crack initiation resistance. Nevertheless, BSE
 503 (Back Scattering Electron) analyses performed on one of the defects did not reveal any
 504 particular chemical constituent which tends to exclude this hypothesis.



505
506

Figure 15 - Surface imperfection roughness - a) EDM ; b) Abrasive machine

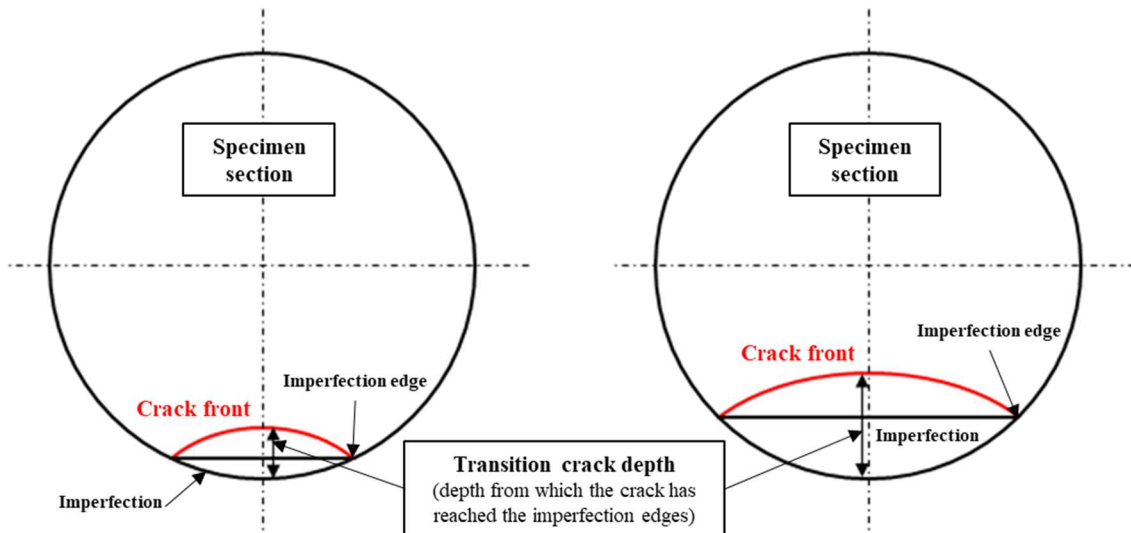
507 Furthermore, a comparison of the 304L initiation results with literature data has been carried
 508 out. As expected, initiation times appear to be significantly reduced in the presence of surface
 509 imperfection when compared with virgin specimens [7, 28]. For the strain amplitudes
 510 considered here, it appears that initiation represents an important part of the total fatigue life. A
 511 recent study [7] conducted under air at room temperature confirms the impact of the presence
 512 of a surface imperfection on crack initiation. As an example, the fraction of the lifetime
 513 represented by initiation for specimens without imperfection is respectively 32% and 31% at
 514 $\Delta\varepsilon_t/2 = 0.2\%$ and 0.3% . It should be noted that the initiation proportion is significantly lower at
 515 $\Delta\varepsilon_t/2 = 0.6\%$, reaching only 8 to 15% of the total lifetime. However, these results are not directly
 516 comparable with those of the present study. Indeed, in Ould Amer's work [7], initiation is
 517 associated with the nucleation of a crack with a 100 μm surface length while the initiation as
 518 defined in this study is associated to a depth of 100 μm . A 100 μm surface crack length is
 519 associated with a depth which obviously depends on the crack front shape, but which is very
 520 likely less than 100 μm (see figure 8). Thus, the initiation proportion from Ould Amer's work

521 mentioned above would probably be higher if the same initiation criterion, i.e. the nucleation
522 of 100 μm -depth crack, were considered.

523 *4.2. Short crack effect and steady-state propagation threshold*

524 The distinction of a micropropagation phase presenting a different fatigue crack growth rate
525 evolution that the one observed for long cracks is a well-known phenomenon in fatigue. The
526 propagation of so-called short cracks has been the subject of numerous studies. Their particular
527 behavior compared to long cracks is generally attributed to miscellaneous factors such as
528 microstructure, environment or again crack closure [29]. In austenitic stainless steels, this
529 phenomenon has been investigated by several authors [7, 19, 20, 30, 31]. Some of them [7, 19,
530 20] have highlighted the presence of a short crack propagation stage in large scale yielding
531 conditions. These latter studies have been carried out on flawless specimens in contrast to the
532 present study. There is therefore a "short crack" effect, independently of the presence of
533 imperfections. In his study on the 304L, Ould Amer [7] has distinguished three propagation
534 domains: the first two ones, corresponding respectively to the microstructural and physical short
535 cracks evolution, can be associated with the micropropagation stage while a third domain is
536 assimilated to the propagation of long cracks. During the first two propagation stages, the author
537 shows a significant fluctuation in the propagation rates. The particular crack evolution in this
538 micropropagation phase is attributed to microstructural effects. The grain boundaries and grain
539 orientation are identified as the main causes of the observed crack growth fluctuations.
540 Actually, grain boundaries act as microstructural barriers that can cause significant
541 deceleration. Strong disorientation between adjacent grains can also lead to a decrease in the
542 propagation rate.

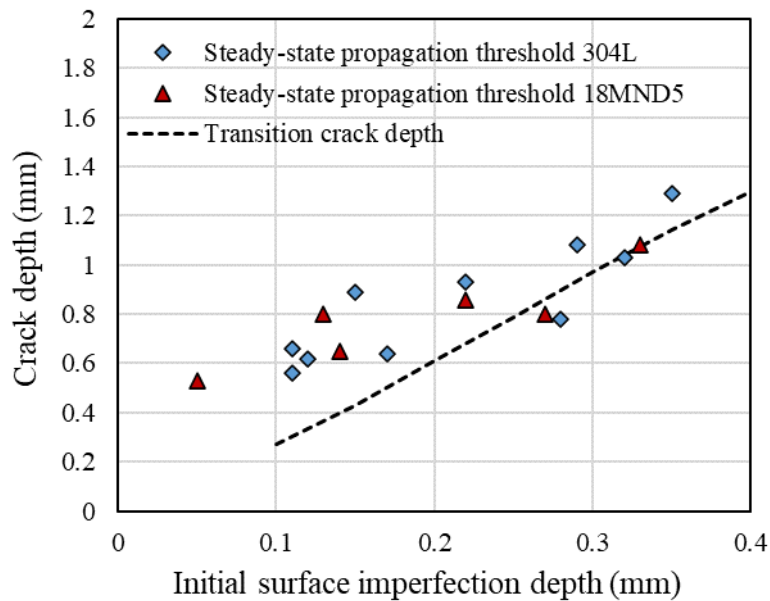
543 In the context of this study, in addition to the above-mentioned microstructural effects, it has
544 been clearly shown that the micropropagation domain is strongly dependent on the surface
545 imperfection presence. Actually, the strain concentration induced by the surface imperfections
546 seems to influence the propagation rates during the micropropagation phase as it has been
547 described in the results section. Moreover, in this propagation domain, the crack growth rate
548 could also be affected by multi-cracking phenomena previously mentioned. It has been shown
549 (figure 5) that, in the early stages of propagation, the crack front shape is irregular and it adopts
550 a semi-elliptical shape mainly after propagating from the initial surface imperfection edge.
551 Then, the emergence of the steady-state propagation regime previously defined may be linked
552 with the end of multi-cracking and coalescence phenomena and the presence of a fully semi-
553 elliptical crack. Estimations from crack growth rates data have been performed on both 304L
554 and 18MND5 in order to identify the appearance of the steady-state propagation regime. The
555 results are presented in figure 17 and compared with the evolution of the crack depth when it
556 separates from the initial surface imperfection. This characteristic crack depth, which will be
557 called "transition depth" here for simplicity sake, is based on the experimental data related to
558 the crack front shape evolution. This "transistion crack depth" concept is illustrated in figure
559 16.



560

561 **Figure 16 - Schematic illustration of the “transition crack depth” (two examples shown with different**
 562 **initial imperfection depths)**

563 The comparison between the steady-state propagation threshold and the transition depth
 564 suggests that these parameters could be potentially linked to each other. Moreover, the
 565 correlation between the data from the two materials seems to indicate that the particular
 566 evolution of the fatigue crack growth rates and the steady-state regime onset are rather
 567 mechanically-driven than microstructurally controlled. Indeed, the microstructures of the two
 568 steels considered in this study are fundamentally different.



569

570 **Figure 17 - Comparison of the evolution of the steady-state propagation regime threshold for 304L and**
 571 **18MND5 steels as a function of the initial imperfection depth with the evolution of the “transition crack**
 572 **depth” evolution**

573

574

575

576 **Conclusions**

577 The influence of the presence of surface imperfections on the fatigue strength of two steels has
578 been studied here on the basis of uni-axial fatigue tests carried out in total strain amplitude
579 control. A particular attention has been paid to assess the respective contribution of crack
580 initiation and propagation from the artificially introduced imperfections in the observed fatigue
581 life by implementing the electrical potential monitoring method in order to quantify the
582 initiation durations and the crack growth rates.

583 The main results can be summarized as follows :

- 584 - The analysis of crack initiation in the 304L, with respect to the threshold criterion
585 defined in the present study (1% variation of $V/V_0 \approx 100 \mu\text{m}$ crack), has shown that in
586 the presence of imperfection, the propagation stage represents the main part of the
587 fatigue life. The exploitation of the data for the 18MND5 steel confirms this statement.
588 In addition, for the 304L, the proportion of initiation is dependent on the initial
589 imperfection depth, in particular at lower strain amplitudes. This latter result is not
590 clearly evidenced for the low alloy steel.
- 591 - An analysis of the fatigue crack propagation rates, derived from electrical potential
592 monitoring, has been proposed. Two propagation domains were distinguished: a first
593 one, assimilable to the micropropagation phase previously defined between the
594 initiation threshold and depths varying approximately between 0.6 and 1.3 mm. This
595 phase is strongly dependent on the initial surface imperfection. The second stage,
596 qualified as a steady-state regime, is characterised by a regular evolution independent
597 on the initial conditions, especially the imperfection depth.
- 598 - Concerning the fatigue lifetime, the results indicate that the presence of surface
599 imperfections induces a significant reduction in fatigue life, even for shallow depths
600 close to $100 \mu\text{m}$. The imperfection depth appears to be the main parameter governing
601 the fatigue life. Finally, the fatigue life abatements are due to a combination of two
602 phenomena, first, a systematic reduction in crack initiation and secondly, the high crack
603 growth rates in the micropropagation stage especially for the deepest imperfections.

604 Experimental data obtained in the framework of this study on crack initiation and propagation
605 should now be further exploited in view of the proposal of a predictive method. In particular
606 mechanical parameters such as ΔJ or ΔK_e [32-33], which can be used in the context of large-
607 scale plasticity of this work, will be considered as driving force parameters to analyze the
608 fatigue crack growth data from the different tests.

609 **Acknowledgements**

610 The author acknowledges the Région Nouvelle-Aquitaine as well as the Framatome company
611 for their financial support. Special thanks are also extended to the entire laboratory technical
612 staff of the Pprime ENDO group for their assistance during the fatigue tests as well as for the
613 specimen preparation.

614

615

616

617 **References**

- 618 [1] Doremus, L., Cormier, J., Villechaise, P., Henaff, G., Nadot, Y., Pierret, S., 2015a. Influence
619 of residual stresses on the fatigue crack growth from surface anomalies in a nickel-based
620 superalloy. *Mater. Sci. Eng. -Struct. Mater. Prop. Microstruct. Process.* 644, 234–246.
621 <https://doi.org/10.1016/j.msea.2015.07.077>
- 622 [2] Gourdin, S., Cormier, J., Henaff, G., Nadot, Y., Hamon, F., Pierret, S., 2017. Assessment
623 of specific contribution of residual stress generated near surface anomalies in the high
624 temperature fatigue life of a Rene 65 superalloy. *Fatigue Fract. Eng. Mater. Struct.* 40, 69–80.
625 <https://doi.org/10.1111/ffe.12475>
- 626 [3] Cini, A., Irving, P.E., 2010. Transformation of defects into fatigue cracks; the role of Kt
627 and defect scale on fatigue life of non-pristine components. *Procedia Eng.* 2, 667–677.
628 <https://doi.org/10.1016/j.proeng.2010.03.072>
- 629 [4] Jiang, Q., Sun, C., Liu, X., Hong, Y., 2016. Very-high-cycle fatigue behavior of a structural
630 steel with and without induced surface defects. *Int. J. Fatigue* 93, 352–362.
631 <https://doi.org/10.1016/j.ijfatigue.2016.05.032>
- 632 [5] Inchekel, A., Talia, J.E., 1994. Effect of scratches on the fatigue behavior of an Al-Li alloy.
633 *Fatigue Fract. Eng. Mater. Struct.* 17, 501–507
- 634 [6] De Baglion, L., Mendez, J., 2010. Low cycle fatigue behavior of a type 304L austenitic
635 stainless steel in air or in vacuum, at 20 °C or at 300 °C: Relative effect of strain rate and
636 environment. *Procedia Eng., Fatigue* 2010 2, 2171–2179.
637 <https://doi.org/10.1016/j.proeng.2010.03.233>
- 638 [7] Ould Amer, A., 2014. Endommagement à différentes échelles d'un acier austénitique
639 inoxydable en fatigue à amplitude constante et variable. ENSTA ParisTech
- 640 [8] Poulain, T., Mendez, J., Hénaff, G., de Baglion, L., 2017. Analysis of the ground surface
641 finish effect on the LCF life of a 304L austenitic stainless steel in air and in PWR environment.
642 *Eng. Fract. Mech.* 185, 258–270. <https://doi.org/10.1016/j.engfracmech.2017.05.043>
- 643 [9] Petitjean, S., 2003. Influence de l'état de surface sur le comportement en fatigue à grand
644 nombre de cycles de l'acier inoxydable austénitique 304L. Thèse de l'Université de Poitiers
- 645 [10] Clark, G., Knott, J.F., 1975. Measurement of fatigue cracks in notched specimens by means
646 of theoretical electrical potential calibrations. *J. Mech. Phys. Solids* 23, 265–276
- 647 [11] Johnson, H.H., 1965. Calibrating the Electric Potential Method for Studying Slow Crack
648 Growth. *Mater. Res. Stand.* 5, 442
- 649 [12] Smith, R.A., Cameron, A.D., 1984. A three dimensional wax analogue for the calibration
650 of the electrical potential technique of crack growth monitoring, in: Valluri, S.R., Taplin,
651 D.M.R., Rao, P.R., Knott, J.F., Dubey, R. (Eds.), *Fracture* 84. Pergamon, pp. 3371–3376.
652 <https://doi.org/10.1016/B978-1-4832-8440-8.50362-8>
- 653 [13] Ritchie, R.O., Bathe, K.J., 1979. On the calibration of the electrical potential technique for
654 monitoring crack growth using finite element methods. *Int. J. Fract.* 15, 47–55

- 655 [14] Gandossi, L., Summers, S.A., Taylor, N.G., Hurst, R.C., Hulm, B.J., Parker, J.D., 2001.
656 The potential drop method for monitoring crack growth in real components subjected to
657 combined fatigue and creep conditions: application of FE techniques for deriving calibration
658 curves. *Int. J. Press. Vessels Pip.* 78, 881–891. [https://doi.org/10.1016/S0308-0161\(01\)00103-](https://doi.org/10.1016/S0308-0161(01)00103-X)
659 X
- 660 [15] Doremus, L., Nadot, Y., Henaff, G., Mary, C., Pierret, S., 2015b. Calibration of the
661 potential drop method for monitoring small crack growth from surface anomalies - Crack front
662 marking technique and finite element simulations. *Int. J. Fatigue* 70, 178–185.
663 <https://doi.org/10.1016/j.ijfatigue.2014.09.003>
- 664 [16] Lambourg, A., Henaff, G., Nadot, Y., Gourdin, S., Pujol d'Andrebo, Q., Pierret, S., 2020.
665 Optimization of the DCPD technique for monitoring the crack propagation from notch root in
666 localized plasticity. *Int. J. Fatigue* 130, 105228. <https://doi.org/10.1016/j.ijfatigue.2019.105228>
- 667 [17] Enmark, M., Lucas, G., Odette, G., 1992. An Electric-Potential Drop Technique for
668 Characterizing Part-Through Surface Cracks. *J. Nucl. Mater.* 191, 1038–1041.
669 [https://doi.org/10.1016/0022-3115\(92\)90632-U](https://doi.org/10.1016/0022-3115(92)90632-U)
- 670 [18] Ikeda, K., Yoshimi, M., Miki, C., 1991. Electrical potential drop method for evaluating
671 crack depth. *Int. J. Fract.* 47, 25–38
- 672 [19] De Baglion, L., 2011. Comportement et endommagement en fatigue oligocyclique d'un
673 acier inoxydable austénitique 304L en fonction de l'environnement (vide, air, eau primaire
674 REP) à 300°C. Thèse Ensma, Poitiers
- 675 [20] Poulain, T., 2015. Fatigue oligocyclique d'un acier inoxydable austénitique 304L :
676 influence de l'état de surface et de signaux de chargement en milieu eau primaire REP
- 677 [21] Akamatsu M., Chevallier E., 2001. Caractérisation chimique et mécanique des
678 matériaux approvisionnés pour l'étude du comportement en fatigue des aciers inoxydables
679 austénitiques, Projet HT-42/00/020/A, EDF
- 680 [22] Ljustell, P., 2011. The Effect of Large Scale Plastic Deformation on Fatigue Crack Length
681 Measurement with the Potential Drop Method. *J. Test. Eval.* 39, 985–1002.
682 <https://doi.org/10.1520/JTE103532>
- 683 [23] Tarnowski, K.M., Davies, C.M., Dean, D.W., Nikbin, K.M., 2015. The Influence of
684 Plasticity on Crack Length Measurements Using the Potential Drop Technique, in: Kang, J.,
685 Jablonski, D., Dudzinski, D. (Eds.), *Evaluation of Existing and New Sensor Technologies for*
686 *Fatigue, Fracture and Mechanical Testing*. ASTM International, 100 Barr Harbor Drive, PO
687 Box C700, West Conshohocken, PA 19428-2959, pp. 73–96.
688 <https://doi.org/10.1520/STP158420140055>
- 689 [24] Tarnowski, K.M., Dean, D.W., Nikbin, K.M., Davies, C.M., 2017. Predicting the influence
690 of strain on crack length measurements performed using the potential drop method. *Eng. Fract.*
691 *Mech.* 182, 635–657. <https://doi.org/10.1016/j.engfracmech.2017.06.008>
- 692 [25] Maiya, P., 1979. Effects of Notches on Crack Initiation in Low-Cycle Fatigue. *Mater. Sci.*
693 *Eng.* 38, 289–294. [https://doi.org/10.1016/0025-5416\(79\)90134-4](https://doi.org/10.1016/0025-5416(79)90134-4)

- 694 [26] Carpinteri, A., 1993. Shape change of surface cracks in round bars under cyclic axial
695 loading. *Int. J. Fatigue* 15, 21–26
- 696 [27] NUREG/CR-6909 Rev. 1. Effect of LWR Water Environments on the Fatigue Life of
697 Reactor Materials
- 698 [28] Maiya, P.S., 1975. Considerations of crack initiation and crack propagation in low-cycle
699 fatigue. *Scr. Metall.* 9, 1141–1146. [https://doi.org/10.1016/0036-9748\(75\)90394-4](https://doi.org/10.1016/0036-9748(75)90394-4)
- 700 [29] Suresh, S., Ritchie, R.O., 1984. Propagation of short fatigue cracks. *Int. Met. Rev.* 29, 445–
701 475
- 702 [30] Obrtlík, K., Polak, J., Hajek, M., Vasek, A., 1997. Short fatigue crack behaviour in 316L
703 stainless steel. *Int. J. Fatigue* Vol. 19, No. 6, pp. 471–475
- 704 [31] Blochwitz, C., Jacob, S., Tirschler, W., 2008. Grain orientation effects on the growth of
705 short fatigue cracks in austenitic stainless steel. *Materials Science and Engineering A* 496 59–
706 66
- 707 [32] Dowling, N.E., 1976. Geometry effects and the J-integral approach to elastic-plastic
708 fatigue crack growth, in: *Cracks and Fracture*. ASTM International
- 709 [33] Kamaya, M., 2015. Low-cycle fatigue crack growth prediction by strain intensity factor.
710 *Int. J. Fatigue* 72, 80–89. <https://doi.org/10.1016/j.ijfatigue.2014.11.002>

711

712 **Shortened version of the abstract used for the online submission**

713 The impact of a controlled surface imperfection on the low-cycle fatigue life in two different
714 steels is investigated. After introduction of a single imperfection with a depth varying from 50
715 to 350 μm in cylindrical samples, fatigue tests were conducted under fully-reversed total axial
716 strain control in air at ambient temperature. It is shown that the fatigue life is significantly
717 reduced, even in presence of small imperfections. In addition, the use of the potential drop
718 methods provided an assesment of the initiation life and the determination of crack growth rates.
719 Two characteristic crack growth domains were thus identified.